Hindawi
Shock and Vibration
Volume 2022, Article ID 8094392, 14 pages
https://doi.org/10.1155/2022/8094392

Research Article

A Small-Amplitude Control Method of the Nonlinear Energy Sink Vibration Absorption System

Qingchao Yang,[1] Shuang Li,[2] and Jingjun Lou[1]

[1]*College of Naval Architecture and Ocean Engineering, Naval University of Engineering, No. 717, Hanshuiqiao Street, Qiaokou District, Wuhan 430033, China*
[2]*Unit of 32801 People's Liberation Army, No. 28, Fuxing Road, Haidian District, Beijing 100082, China*

Correspondence should be addressed to Jingjun Lou; 1352363409@qq.com

Received 13 May 2022; Revised 13 October 2022; Accepted 26 November 2022; Published 6 December 2022

Academic Editor: Stefano Marchesiello

The nonlinear energy sink (NES) is an effective method to weaken or eliminate the line spectra feature of ship machinery equipment. However, due to the strong nonlinearity of the NES, there are multistable attractors in the NES vibration absorption system. Moreover, when the excitation characteristics or working conditions of the mechanical equipment change, the NES may migrate from the small-amplitude motion state to the large-amplitude motion state, resulting in a high-amplitude solitary branch response and thereby lowering its vibration absorption efficiency. In this study, the small-amplitude control of the NES nonlinear vibration absorption system has been studied by using the open-loop-plus-nonlinear-closed-loop (OLPNCL) method. First, the dynamic equation of the NES nonlinear vibration-absorbing system was formulated, and its global behavior was analyzed. The regulations of global features and coexisting attractors were found out. Second, the migration between different attractors was carried out under the OLPNCL control, which can ensure that the system always works at the lowest line spectrum intensity and the best overall vibration absorption performance. Finally, the simulation results verify the feasibility and effectiveness of the OLPNCL method and achieve effective vibration absorption in the low-frequency range and line spectrum control under variable operating conditions.

1. Introduction

With continual interest in expanding the performance envelope of engineering systems, nonlinear components are increasingly utilized in real-world applications. A recent trend in the technical literature is to exploit nonlinear dynamical phenomena instead of avoiding them [1–3]. Nonlinearity is also more and more utilized for vibration mitigation. The applications of nonlinear vibration absorbers to eliminate undesirable vibration of linear structures have been examined by numerous researchers [4–6]. Recent developments in passive nonlinear vibration absorbers include the NES [7, 8] and nonlinear viscous dampers [9, 10]. Actually, in view of narrow bandwidth, the linear tuned mass damper or dynamic vibration absorber can be ineffective when the primary structure exhibits frequency–energy-dependent nonlinear oscillations [11]. Many researchers addressed the vibration mitigation of nonlinear mechanical systems using nonlinear dynamical absorbers [12–14].

As it is known, the NES is a candidate for nonlinear vibration absorbers for vibration mitigation of nonlinear mechanical structures. An NES is commonly composed of a small mass with respect to the primary structure, a viscous damper, and a spring with zero or quasi-zero linear stiffness but strong nonlinear stiffness. Thanks to the essential nonlinearity, the kinetic energy of the primary structure can be transferred, localized, and diminished within the NES over a broad frequency spectrum, which is known as targeted energy transfer (TET) [15]. It has gained considerable interest in a range of applications [6], including vibration attenuation in civil engineering [16, 17], vibration

suppression in mechanical engineering [18, 19], vibration mitigation in aeronautics and astronautics [20, 21], and energy harvesting with NESs [22, 23].

However, Dudkowski et al. [24] studied hidden attractors in dynamic systems and found that hidden attractors have small basins of attractions, and the system evolution on them is very sensitive towards external perturbations (noise), initial conditions, and small changes in the system's parameters. Typically, even small perturbations can lead to unexpected switches to a different attractor. Pisarchik and Hramov [25] pointed out that multistable systems are very sensitive to parameter perturbations that can cause qualitatively different behavior, especially near the bifurcation point, where a tiny change in a control parameter may result in the emergence of a large number of attractors. Meanwhile, the amplitude of coexistent attractors varies greatly, so the performance of vibration isolation highly depends on initial conditions and system parameters, which means that it is possible to jeopardize the quality of vibration isolation and even amplify the vibration. A vibration system with multiple interference sources is highly prone to mitigating from a small-amplitude to a large-amplitude motion state, thus lowering the vibration absorption efficiency of the NES. Therefore, a control method is urgently needed to quickly transform the motion of other attractors to the minimum vibration of the foundation. The global control method is developed from open loop and closed loop to open-plus-closed-loop and open-plus-nonlinear-closed-loop (OPNCL) [26]. The former three methods have some shortcomings, such as overstrict initial value limit and overcomplicated basins of migrating range determination. Starosvetsky and Gendelman [27] designed an NES with a properly tuned piecewise-quadratic damping element, which allowed the complete elimination of undesirable periodic regimes under certain parameter conditions. Eason [28] added an adaptive length pendulum (ALP) device to the NES structure and adjusted the pendulum length through the semiactive control technology to make the system out of the regions of solitary branch response. Liu et al. [11] designed an NES structure with adjustable parameters using two inclined spring-damper elements, which could remove the high-amplitude solitary branch response by adjusting the initial inclination angle of the spring-damper elements. Zang et al. [29] proposed a lever-type NES, which could suppress the solitary branch response by adjusting the fulcrum position of the lever. But so far, the above-mentioned control methods still have some technical challenges, such as high control energy consumption and strict requirements for the stability of the control track. If we hope to realize that the large-amplitude periodic attractor migrates to the small-amplitude chaotic attractor accurately and quickly by smaller control energy and fewer control numbers, some further research still needs to be carried out.

In this paper, a migration control algorithm based on the deterministic relationship between different attractors and their basins of attraction is introduced, which can quickly migrate the mechanical equipment response to a small-amplitude attractor when it is at a large-amplitude attractor or maintains it at a small-amplitude attractor when it has already been so. The proposed method can improve the stability of the NES and enhance its engineering application value.

The rest of this paper is organized as follows: In Section 2, the dynamic model of the NES vibration-absorbing system is established, and the global properties of the system are obtained using the cell mapping method [30–32]. In Section 3, the migration control method for multiple attractors in nonlinear systems is introduced in detail. Finally, in Section 4, simulation calculations are carried out for the migration control between different periodic attractors, periodic attractors, and chaotic attractors, and the effectiveness of the migration control method is verified.

2. Dynamic Modeling and Global Behavior Analysis of the NES Vibration Absorption System

2.1. Dynamic Modeling. The dynamics model of a general dynamic vibration absorber is built for the mechanical equipment coupled with an NES, as shown in Figure 1.

The main system is composed of m_1, k_1, and λ_1, among which m_1 is the mechanical equipment to be damped, which is connected to the rigid base through the linear spring with stiffness k_1 and damper λ_1. The NES, comprising mass m_2, stiffness k_2, and damper λ_2, is installed on the upper layer of the mechanical equipment and coupled with the mechanical equipment. When the external excitation signal f_b is applied to the mechanical equipment, the vertical displacements generated by the mechanical equipment and the NES are x_1 and x_2, respectively. The NES satisfies the cubic stiffness characteristic, and the restoring force of the nonlinear spring is $f_{\mathrm{NES}} = k_2(x_2 - x_1)^3$.

The dynamics equations of the system are

$$\left\{ m_1\ddot{x}_1 + \lambda_1\dot{x}_1 + k_1x_1 + \lambda_2(\dot{x}_1 - \dot{x}_2) + k_2(x_1 - x_2)^3 = f_b, m_2\ddot{x}_2 + \lambda_2(\dot{x}_2 - \dot{x}_1) + k_2(x_2 - x_1)^3 = 0. \right. \tag{1}$$

The periodic operation of the ship hydraulic pump, air compressor, and other mechanical equipment will generate mechanical vibration, and the vibration will excite the hull through the transmission path such as the floating raft and the base to form the line spectrum component in the underwater radiated noise. Therefore, we focus on the study of the vibration suppression effect of nonlinear energy wells under harmonic excitation.

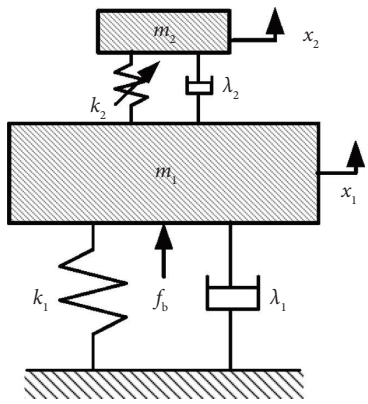

Figure 1: The dynamics model of the NES vibration absorption system.

The excitation form follows the equitation $f_b = F\ \cos\ (\Omega T)$, in which F is the amplitude of the harmonic excitation and Ω is the frequency of excitation.

The dimension of length is introduced, given by $l_0 = (m_1 g/k_1)$, and l_0 corresponds to the static deformation of the linear spring k_1 under the action of the mass m_1, and dimensionless transformations are performed:

$$t = \Omega_1 T, \Omega_1 = \sqrt{\frac{k_1}{m_1}}, z_1 = \frac{x_1}{l_0}, z_2 = \frac{x_2}{l_0}. \tag{2}$$

The dimensionless dynamics equations of the system under the condition of harmonic excitation can be obtained as

$$\begin{cases} \ddot{z}_1 + \xi_1 \dot{z}_1 + z_1 + \xi_2 (\dot{z}_1 - \dot{z}_2) + \beta (z_1 - z_2)^3 = f\ \cos\ \omega\, t, \ddot{z}_2 + \dfrac{\xi_2}{\varepsilon} (\dot{z}_2 - \dot{z}_1) + \dfrac{\beta}{\varepsilon} (z_2 - z_1)^3 = 0. \end{cases} \tag{3}$$

Here,

$$\varepsilon = \frac{m_2}{m_1}, \xi_1 = \frac{\lambda_1}{m_1 \Omega_1}, \xi_2 = \frac{\lambda_2}{m_1 \Omega_1}, \omega = \frac{\Omega}{\Omega_1}, f = \frac{F}{l_0 k_1}, \beta = \frac{k_2 {l_0}^2}{k_1}. \tag{4}$$

Equations in (3) can be rewritten in the form of a space state equation set as

$$\begin{cases} \dot{z}_1 = F_1(\mathbf{x}, t) = y_1, \\ \dot{y}_1 = F_2(\mathbf{x}, t) = -z_1 - \beta (z_1 - z_2)^3 - \xi_1 y_1 - \xi_2 (y_1 - y_2) + f \cos\ \omega\, t, \\ \dot{z}_2 = F_3(\mathbf{x}, t) = y_2, \\ \dot{y}_2 = F_4(\mathbf{x}, t) = -\dfrac{\beta}{\varepsilon} (z_2 - z_1)^3 - \dfrac{\xi_2}{\varepsilon} (y_2 - y_1), \end{cases} \tag{5}$$

where $\mathbf{x} = (z_1, y_1, z_2, y_2)^{\mathrm{T}}$ is the state vector of the system and $\mathbf{F}(\mathbf{x}, t) = [F_1(\mathbf{x}, t), F_2(\mathbf{x}, t), F_3(\mathbf{x}, t), F_4(\mathbf{x}, t)]^{\mathrm{T}}$ is the polynomial.

2.2. Global Bifurcation Analysis. An important prerequisite for realizing the small-amplitude control method of the attractor is an in-depth and comprehensive global bifurcation analysis of the dynamical system. Only in this way, the various attractors in the system can be accurately controlled according to their dynamic characteristics, so as to achieve the ideal control effect. In this study, we focus on the influence of the excitation force amplitude on the global bifurcation behavior and the global bifurcation behavior of mechanical equipment and the NES system, which can provide prior information for the migration control of attractors.

In our study, the 4th Runge–Kutta method is applied, and the simulation software is MATLAB/Simulink. With the integration time set as 1000 periods, the response

value within 500 periods, after the system motion state stabilizes, is used as the data source. The excitation force amplitude f is controlled to change within a large parameter range, $0 \le f \le 30$, with a step length of $\Delta f = 0.01$, and the following parameters are set: $\xi_1 = 0.1$, $\xi_2 = 0.01$, $\beta = 0.3$, $\varepsilon = 0.6$, and $\omega = 1.6$. As shown in Figure 2, the global bifurcation diagram and the maximum Lyapunov exponent spectrum of the NES system is in the parameter range of $f = 0 \sim 30$. It can be seen from Figure 2, regardless of the forward continuation or backward continuation, the system exhibits very complex dynamic characteristics when the amplitude of the excitation force changes within a large parameter range. Periodic motion, quasiperiodic motion, and chaotic motion all exist in the system, in which stable periodic motion takes the dominant position, while quasiperiodic motion and chaotic motion are mainly located in the amplitude range of certain excitation forces. Therefore, by changing the excitation amplitude, the NES vibration absorption system can realize the migration of different motion states. In addition, multistable attractors coexist in the system with multiple parameter ranges, such as there are two period-1 attractors that coexist when $0.19 \le f \le 1.11$, one period-1 attractor and one quasiperiodic attractor when $10.5 \le f \le 11.86$, one period-3 attractor and one chaotic attractor when $19.34 \le f \le 19.62$, and one period-2 attractor and one chaotic attractor when $25.19 \le f \le 26.01$.

The coexistence of multistable attractors is determined by the multivalued nature of the nonlinear system, which enables each attractor to have its corresponding basin of attraction. Therefore, when the excitation force amplitude f is in a typical interval, the cell mapping method should be used to further determine the corresponding relationship between the attractors and their basins of attraction in the NES system.

In the typical interval I, the excitation force amplitude f is set to 0.68. There are two stable period-1 attractors in the system response, whose phase trajectories are shown in Figure 3. As illustrated, attractor A_1 has a larger amplitude than attractor A_2. According to the cell mapping method, if the analysis plane $-2 \le z_1 \le 2$ and $-2 \le y_1 \le 2$ are selected, with the initial conditions of the fixed variables z_2 and y_2 both set to be 0, then it can be divided into 100×100 discrete cells (totaling 40,000) as the primitive ones. The number of parallel computing $N_s = 100$, and the calculation results are shown in Figure 4(a). In the figure, the position of attractor A_1 is marked by "," and the red areas are its basins of attraction; the position of attractor A_2 is marked by "," and the cyan areas represent its basins of attraction. It can be seen that the area of A_1's basins of attraction occupies 86.39% of the entire analysis plane, while for A_2's basins of attraction, the value is 13.61%. However, if the analysis plane selected are $-4 \le z_2 \le 4$ and $-4 \le y_2 \le 4$, with the initial conditions of the fixed variables z_2 and y_2 still set to be 0, the calculation result is shown in Figure 4(b). It can be known that in this analysis plane, A_2's basins only occupy 3.05% of the total area, with the remaining 96.95% occupied by A_1's basins.

In the typical interval II, the excitation force amplitude f is set to 19.5. There is a stable period-3 attractor and a stable chaotic attractor in the system response, whose phase trajectories are shown in Figure 5. If the analysis plane $-8 \le z_1 \le 8$ and $-15 \le y_1 \le 15$ are selected, with the initial conditions of the fixed variables z_2 and y_2 both set to 0, then it can be divided into 200×200 discrete cells (totaling 40,000) as the primitive ones. The number of parallel computing $N_s = 100$, and the calculation results are shown in Figure 6(a). In the figure, the "" represents the position of the period-3 attractor, while the green area represents the position of the chaotic attractor, with the red and cyan areas corresponding to the basins of attraction of the period-3 attractor and the chaotic attractor, respectively. As illustrated in Figure 6(a), in the $z_1 - y_1$ analysis plane, the system response is dominated by chaotic motion; the chaotic attractor's basins of attraction occupy 72.98% of the area of the entire plane, while the period-3 attractor's basins only occupy 27.02%. Additionally, the two attractors are interwoven, and the overall behavior is complicated. If the analysis plane $-12 \le z_2 \le 12$ and $-12 \le y_2 \le 12$ are selected, with the fixed variables $z_2 = 0$ and $y_2 = 0$, the calculation results are shown in Figure 6(b). In the $z_2 - y_2$ analysis plane, the chaotic attractor's basins of attraction occupy 72.98% of the area of the entire plane and the period-3 attractor's basins only occupy 26.76%. Moreover, the fractal boundary of the two attractors' basins of attraction in the analysis plane is not as obvious as in Figure 6(a), which suggests that the system response is sensitive to the initial condition changes of NESs.

3. The Migration Control Method of the Attractor

3.1. Basic Theory of the Migration Control Method. Multivalued nonlinear systems generally exist and belong to multiple attractor subsystems, and each attractor has its own attraction domain. The transport control that realizes the conversion between different attractors is called migration control.

Consider the following nonautonomous continuous nonlinear dynamical system:

$$\frac{\mathrm{d}x}{\mathrm{d}t} = F(x,t) + S(t)K(g,x,t), \ (x \in R^n, g \in R^n), \tag{6}$$

where $F_i(x,t) = \sum_{j_1+j_2+\cdots+j_n=0}^{m} a_{j_1,j_2,\cdots,j_n}^{(i)}(t) x_1^{j_1} x_2^{j_2} \cdots x_n^{j_n}$ $(i = 1, 2, \cdots, n)$ and m is the polynomial degree of $F(x,t)$. We assume that there exists at least one nonzero parameter, for example, $a_{j_1,j_2,\cdots,j_n}^{(i)}(t) \ne 0 \ (1 \le i \le n, j_1 + j_2 + \cdots + j_n = m)$. $S(t)$ is a switching function, $S(t) = 0 \ (t < t_0)$ and $0 < S(t) \le 1 \ (t \ge t_0)$, which will mitigate violent reactions when control action is added. t_0 is the starting time, and when $t < t_0$, the controller does not work, and when $t \ge t_0$,

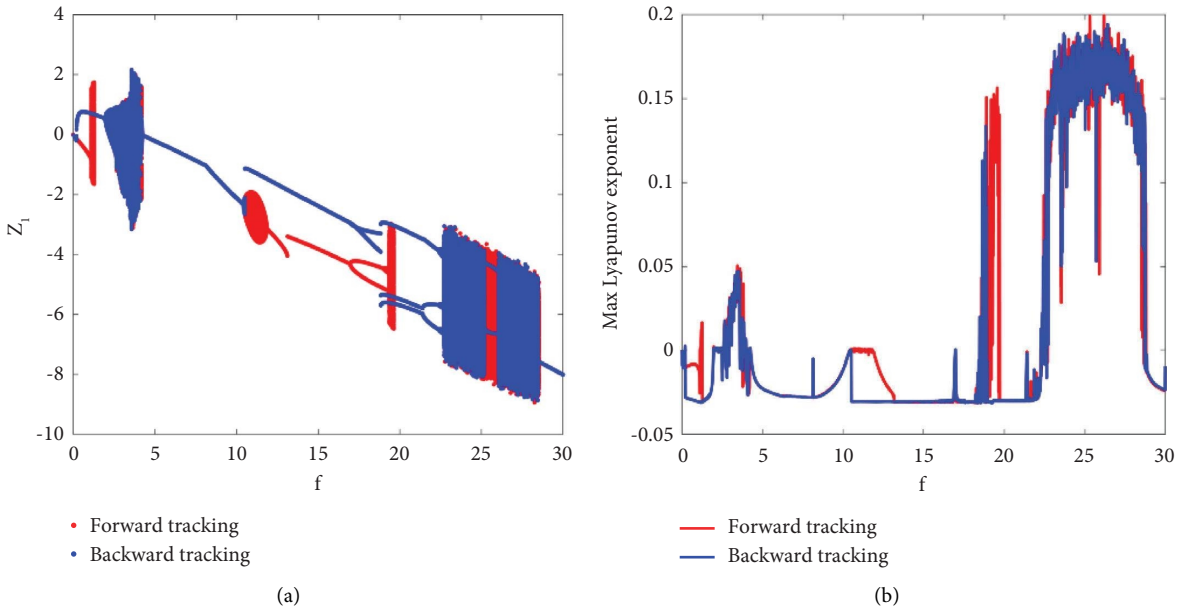

Figure 2: Global bifurcation diagram and the maximum Lyapunov exponent spectrum varying with the excitation amplitude. (a) Global bifurcation diagram. (b) Maximum Lyapunov exponent.

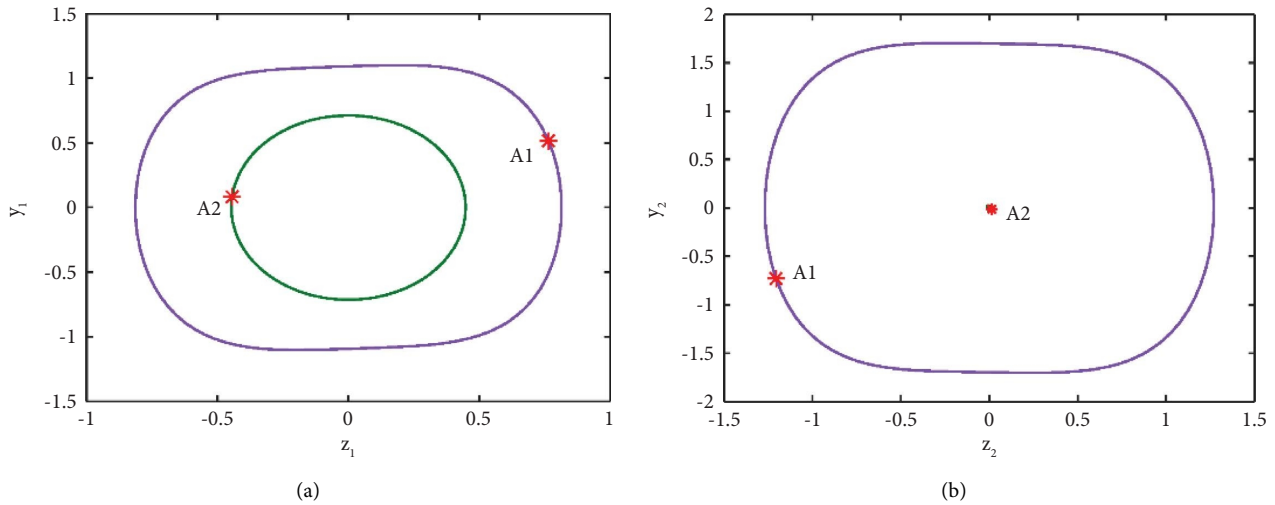

Figure 3: The phase trajectories of the different attractors. (a) The mechanical equipment vibration response. (b) The NES vibration response.

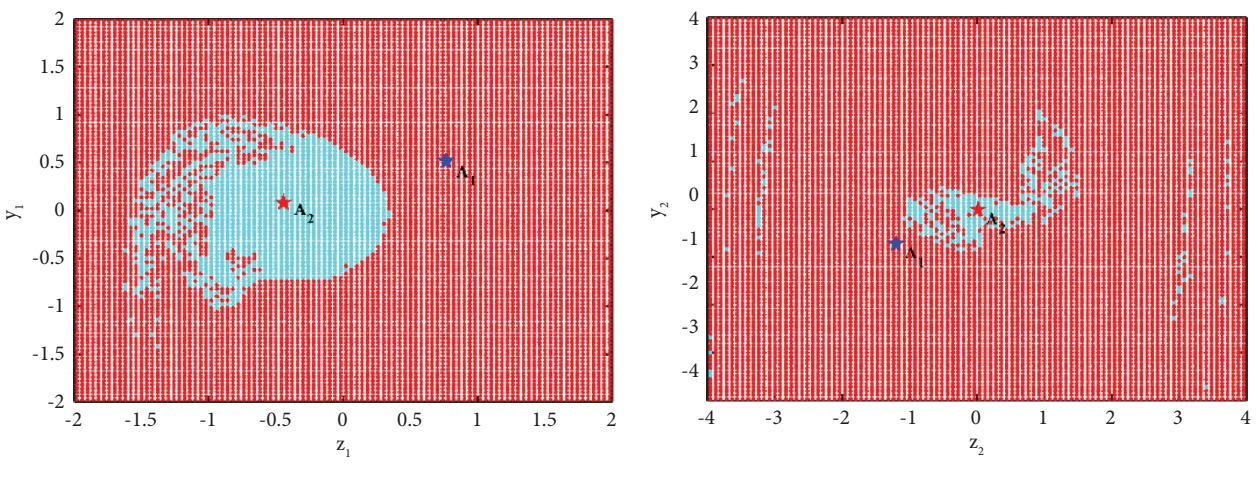

Figure 4: The attractors and their basins of attraction during system response. (a) The $z_1 - y_1$ analysis plane. (b) The $z_2 - y_2$ analysis plane.

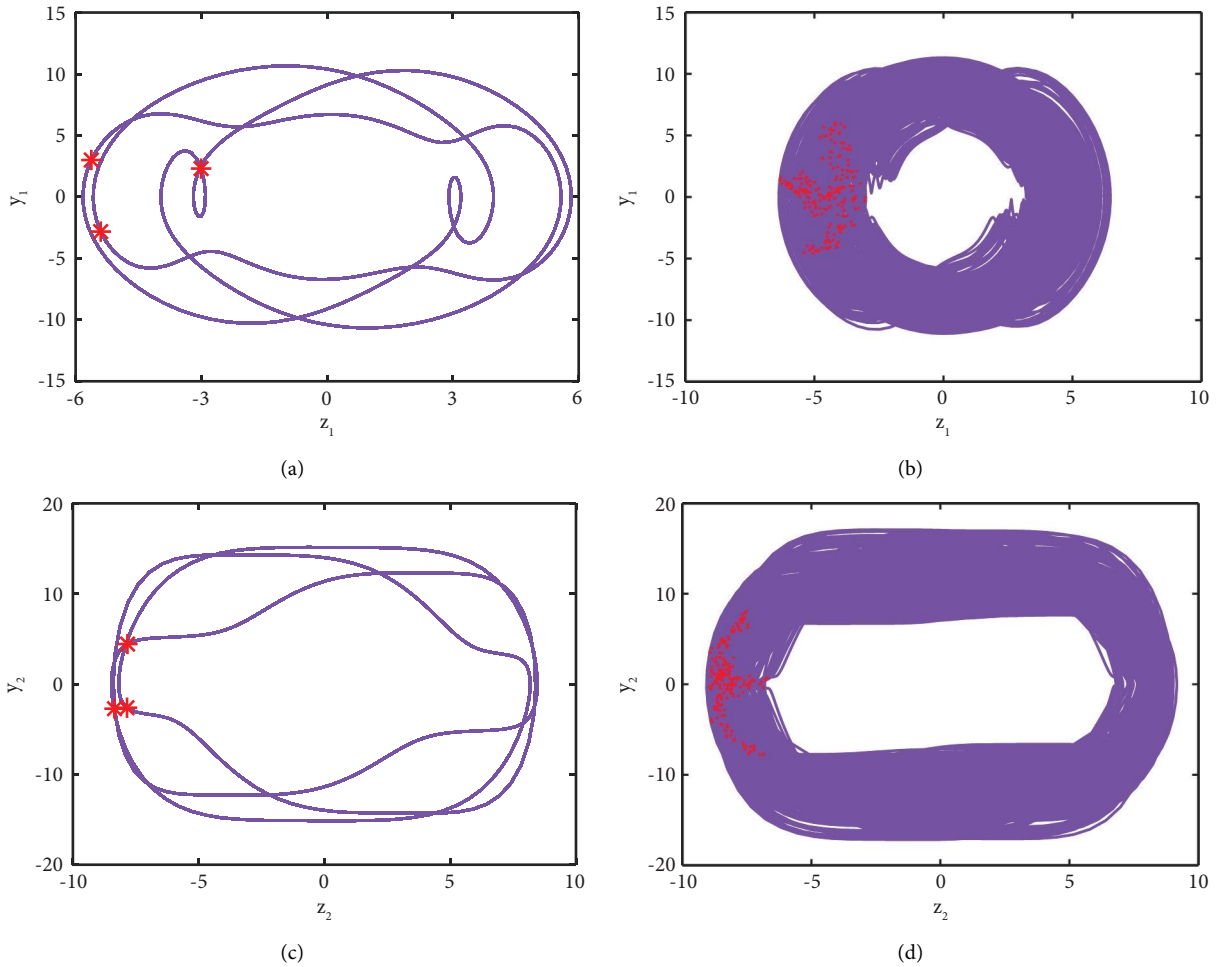

Figure 5: The phase trajectories of the different attractors. (a) The mechanical equipment peroid-3 attractor. (b) The mechanical equipment chaotic attractor. (c) The NES period-3 attractor. (d) The NES chaotic attractor.

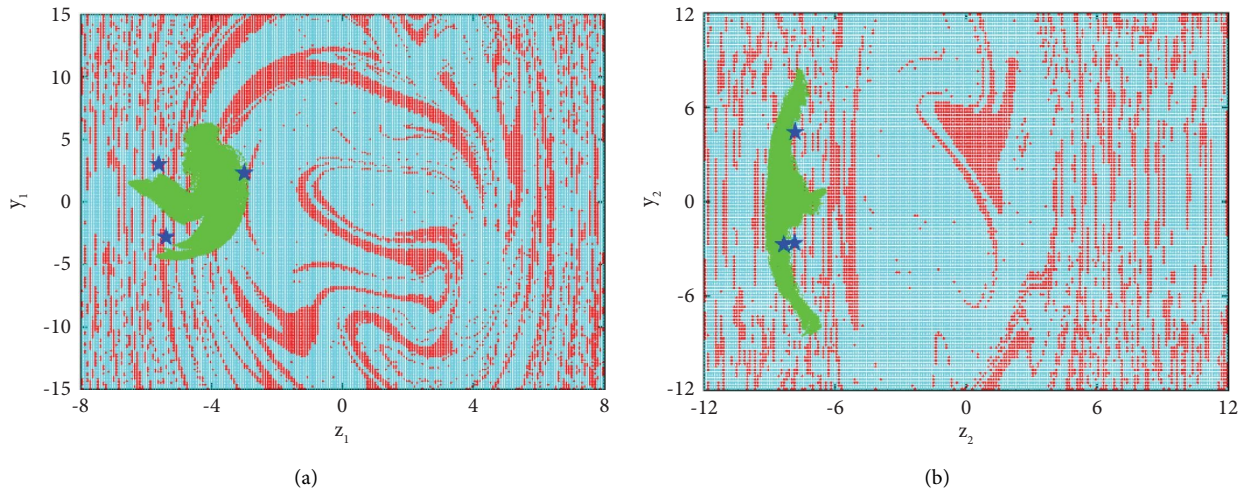

Figure 6: The attractors and their basins of attraction during system response. (a) The $z_1 - y_1$ analysis plane. (b) The $z_2 - y_2$ analysis plane.

the controller begins to work. $K(g,x,t)$ is a control function, associated with $g(t)$ and $x(t)$, where $x(t)$ is the system response and $g(t)$ is the target trajectory function. When the solutions of the system are transported to $g(t)$, it can be obtained as follows:

$$\lim_{t\longrightarrow\infty}\|x(t)-g(t)\|=\lim_{t\longrightarrow\infty}\|e(t)\|=0, \tag{7}$$

where $e(t)$ defines the error between $x(t)$ and $g(t)$. In the process of transport control, the target trajectory $g(t)$ can be a dynamic behavior with any topological properties, but it should be limited to a certain target domain G_k, and $g(t)\in G_k$ and $G_k\cap C_k\neq\varnothing$; C_k is the set of all attractor basins. In addition, transporting basins $BE(g)$ are defined as a set of continuous initial states that the system can be transported to the target trajectory $g(t)$ that satisfy the condition $\lim\|x(t)-g(t)\|=0$. Once the initial state $x(t_0)\in BE^t(\overrightarrow{g})^{\infty}$ is determined and the control is applied, the system can run stably on the target trajectory $g(t)$, and neither further monitoring of the dynamic behavior of the system nor feedback information to stabilize the behavior is required. If a trajectory from an attractor A_1 is transported to another attractor A_2, the only requirement is that the starting state of the transporting trajectory should be chosen in the attractor basin of A_1 and the ending state of the transporting trajectory should be chosen in the attractor basin of A_2. The system trajectory enters the vicinity of the target trajectory $g(t_0)$ to start the transporting control so that the system can run along the target trajectory $g(t)$. After entering the attractor basin of A_2, the controller is turned off and the system can run stably on the attractor A_2.

3.2. The Open-Loop-Plus-Nonlinear-Closed-Loop Control Method. Because the open-loop-plus-linear-closed-loop (OLPLCL) control method has a lower control effect for the system of the high-order polynomial. Therefore, we improve the linear-closed-loop part as nonlinear feedback of "the nonlinear function of the difference between the target orbit variable and the controlled system variable" and propose an open-loop-plus-nonlinear-closed-loop (OLPNCL) control method. The method has been successfully used to achieve generalized chaotic synchronization between the driving system and the response system [33].

Using the OLPNCL control method, equation (7) can be completed, and the control term is

$$K(g,x,t)=\frac{\mathrm{d}g}{\mathrm{d}t}-F(g,t)-C(g,t)e(t)-N(g,x,t), \tag{8}$$

where the matrix $C(g,t)$ is given by $C(g,t)=(\partial F(g,t)/\partial g)-A$ and $A=(a_{ij})$ is constant matrix, whose eigenvalues have negative real parts. $N(g,x,t)$ is the nonlinear closed-loop control action, and its ith element $N_i(g,x,t)$ is given by the following equation:

$$N_i(g,x,t)=\frac{1}{2!}\sum_{j,k=1}^{n}\frac{\partial^2F_i(g,t)}{\partial g_j\partial g_k}e_je_k+\frac{1}{3!}\sum_{j,k,l=1}^{n}\frac{\partial^3F_i(g,t)}{\partial g_j\partial g_k\partial g_l}e_je_ke_l+\cdots+\frac{1}{m!}\sum_{j,k,\cdots,p=1}^{n}\frac{\partial^mF_i(g,t)}{\partial g_j\partial g_k\cdots\partial g_p}e_je_k\cdots e_p,\ m\geq 2,\ i=1,2,\cdots,n. \tag{9}$$

Substituting equations (8) and (9) into (6) of the control system and results in $S(t)=1$, we get

$$\frac{\mathrm{d}e_i}{\mathrm{d}t}=F_i(g+e,t)-F_i(g,t)-\left[\frac{\mathrm{d}F_i(g,t)}{\mathrm{d}g}-A_i\right]e-N_i(g,x,t). \tag{10}$$

$F(g+e,t)$ is expanded in the error (5) for the small e as shown in the following nonlinear approximation:

$$\frac{\mathrm{d}e_i}{\mathrm{d}t}=A_ie+\frac{1}{(m+1)!}\sum_{j,k,\cdots,q=1}^{n}\frac{\partial^{m+1}F_i(g,t)}{\partial g_j\partial g_k\cdots\partial g_q}e_je_k\cdots e_q+\cdots. \tag{11}$$

It is seen that $F(x,t)$ has pth degree polynomials for general dynamics, and $m=p-1$ in the OLPNCL control, which gives the following error equation:

$$\frac{\mathrm{d}e_i}{\mathrm{d}t}=A_ie+\frac{1}{p!}\sum_{j,k,\cdots,q=1}^{n}\frac{\partial^pF_i(g,t)}{\partial g_j\partial g_k\cdots\partial g_q}e_je_k\cdots e_q. \tag{12}$$

The right side of equation (12) does not contain the target function $g(t)$ as the coefficient of e. If m is taken as $m\geq p$, it is found that the error in equation (12) obeys $\dot{e}=Ae(t)$. Since all eigenvalues of A have negative real parts, the Lyapunov direct method is used to prove the asymptotic stability of the zero solution of this equation. Therefore, $BE(g)$ is not being empty sets and any of the basins of transporting associated with $g(t)$ and t_0 is global.

3.3. The Migration Control of Coexisting Attractors in the NES System. The dimensionless dynamic equation of the dynamic vibration absorption system is shown in equation (5),

considering the goal function as $\mathbf{g}(t) = (g_1, g_2, g_3, g_4)^{\mathrm{T}}$ and the error equation as $\mathbf{e} = (e_1, e_2, e_3, e_4)^{\mathrm{T}} = (z_1 - g_1, y_1 - g_2, z_2 - g_3, y_2 - g_4)^{\mathrm{T}}$. It can be found that the equation is similar to equation (6), when equation (5) is added to the OLPNCL action:

$$\begin{Bmatrix} \dot{z}_1 \\ \dot{y}_1 \\ \dot{z}_2 \\ \dot{y}_2 \end{Bmatrix} = \begin{Bmatrix} y_1 \\ F_2(\mathbf{x}, t) \\ y_2 \\ F_4(\mathbf{x}, t) \end{Bmatrix} + S(t) \left\{ \begin{Bmatrix} \dot{g}_1 - g_2 \\ \dot{g}_2 - F_2(\mathbf{g}, t) \\ \dot{g}_3 - g_4 \\ \dot{g}_4 - F_4(\mathbf{g}, t) \end{Bmatrix} + \left[\frac{\partial \mathbf{F}(\mathbf{g}, t)}{\partial \mathbf{g}} - \mathbf{A} \right] \begin{Bmatrix} z_1 - g_1 \\ y_1 - g_2 \\ z_2 - g_3 \\ y_2 - g_4 \end{Bmatrix} \right\} - \mathbf{N}(\mathbf{g}, \mathbf{x}, t), \tag{13}$$

where

$$\frac{\partial \mathbf{F}(\mathbf{g}, t)}{\partial \mathbf{g}} = \begin{bmatrix} 0 & 1 & 0 & 0 \\ -1 - 3\beta(g_1 - g_3)^2 & -\xi_1 - \xi_2 & 3\beta(g_1 - g_3)^2 & \xi_2 \\ 0 & 0 & 0 & 1 \\ \dfrac{3\beta(g_3 - g_1)^2}{\varepsilon} & \dfrac{\xi_2}{\varepsilon} & \dfrac{-3\beta(g_3 - g_1)^2}{\varepsilon} & \dfrac{-\xi_2}{\varepsilon} \end{bmatrix},$$
$$\mathbf{N}(\mathbf{g}, \mathbf{x}, t) = \begin{bmatrix} 0 \\ -3\beta(g_1 - g_3)(e_1 - e_3)^2 - \beta(e_1 - e_3)^3 \\ 0 \\ \dfrac{3\beta(g_1 - g_3)(e_1 - e_3)^2}{\varepsilon} + \dfrac{\beta(e_1 - e_3)^3}{\varepsilon} \end{bmatrix}. \tag{14}$$

The constant matrix $\mathbf{A}$ is taken as a diagonal matrix of eigenvalues with negative real part:

$$\mathbf{A} = \mathrm{diag}(a_{11}, a_{22}, a_{33}, a_{44}) \quad a_{ii} < 0 \quad i = 1, 2, 3, 4. \tag{15}$$

When $S(t) = 1$, the error equation can be obtained as

$$\frac{\mathrm{d}e_i}{\mathrm{d}t} = a_{ii} e_i \quad i = 1, 2, 3, 4. \tag{16}$$

After applying OLPNCL control to the NES system, error $\|\mathbf{e}\|$ can quickly converge to 0, and its transmission domain is global. Therefore, for any smooth target orbit function, as long as $\mathbf{g}(t)$ can connect different attractors' basins of attraction, OLPNCL control can make the response of mechanical equipment migrate from a large-amplitude to a small-amplitude attractor.

4. Numerical Simulation and Analysis

4.1. Migration Control of Different Periodic Attractors. When the parameters are set as $\xi_1 = 0.1$, $\xi_2 = 0.01$, $\beta = 0.3$, $\varepsilon = 0.6$, $\omega = 1.6$, and $f = 0.68$, the system has a large-amplitude attractor with period-1 motion and a small-amplitude attractor with period-1 motion. Figure 7 shows the time history diagrams of different attractors when the initial conditions are (1,0,0,0) (red curve) and (0,0,0,0) (blue curve). In the figure, attractor A_1 has a higher amplitude than attractor A_2.

When OLPNCL control is applied to the system (5) and matrix $\mathbf{A} = \mathrm{diag}(-5, -5, -5, -5)$, target orbit functions $g_1 = 0.25 + 0.5 \sin 0.5t$, $g_2 = 0.5 \cos 0.5t$, $g_3 = 0.25 + 0.5 \sin 0.5t$, and $g_4 = 0.5 \cos 0.5t$. The positions of the target orbits in the phase space are shown in Figure 8, where the red areas are A_1's basins of attraction, the blue areas are A_2's basins of attraction, and the solid green lines represent the target orbits. As illustrated, in $z_1 - y_1$ and $z_2 - y_2$ analysis planes, both the selected target orbits are channels connecting the two attractors' basins. The duration of control applied is set to greater than 300 s (the system has stabilized). When the system response is in A_1's basins, the control is applied, given by function $S(t) = 1$. When the system response migrates to the target orbit and gets into A_2's basins, the control is removed, given by the function $S(t) = 0$.

Under OLPNCL control, the system response phase trajectories are shown in Figure 9. In the figures, the red solid line represents the trajectory of the system before the control is applied, the black solid line represents the transient trajectory

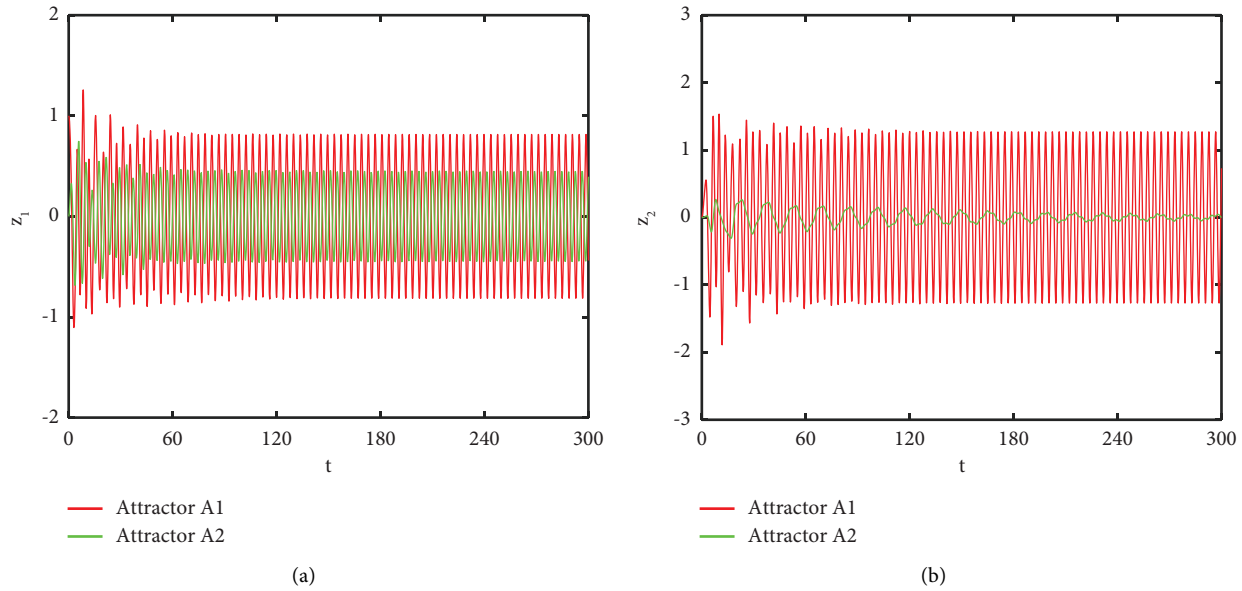

Figure 7: The time history of the system responses under different initial conditions. (a) The mechanical equipment vibration response. (b) The NES vibration response.

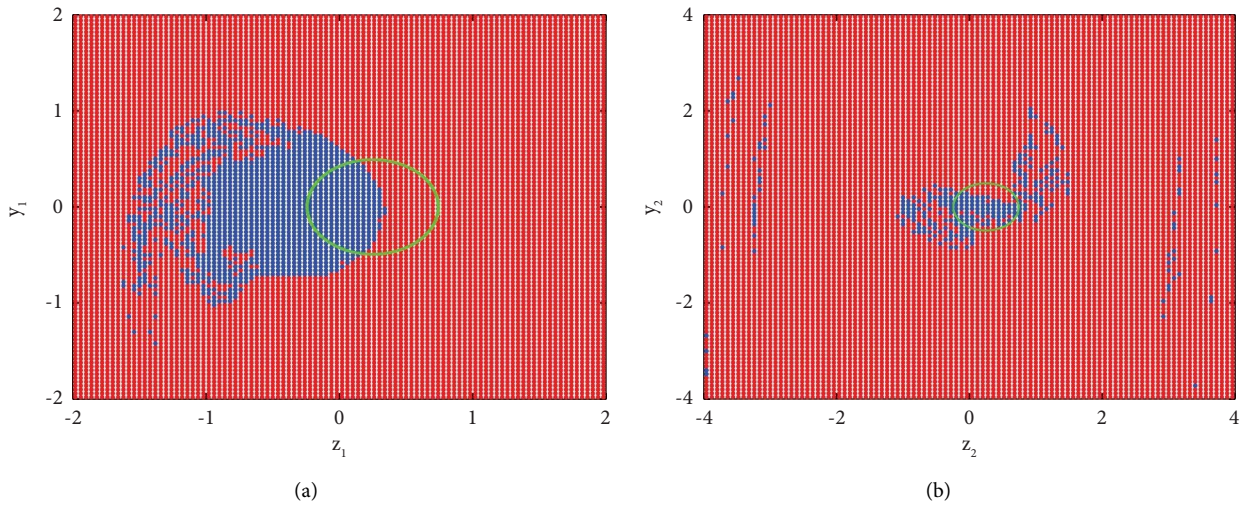

Figure 8: The target orbit's positions in the phase space. (a) The $z_1 - y_1$ analysis plane. (b) The $z_2 - y_2$ analysis plane.

during control application, the green solid line represents the trajectory of the system along the target orbit, the blue solid line represents the system trajectory after the control is removed, and the black arrow represents the changing direction of the system's trajectory before and after the control is applied. Figure 9 shows the change curves of the system's response amplitude with time during the control process. When $t \leq 400$s, the vibrations are large-amplitude; when $400\text{s} < t \leq 540$s, it is the transient process running along the target orbit; when $t > 540$s, the vibrations are small-amplitude. As illustrated by Figures 9 and 10, the vibration responses of the mechanical equipment and NES both can quickly migrate from a large amplitude to a small-amplitude motion state after a short transient process, thereby reducing the vibration amplitude of the mechanical equipment.

4.2. Migration Control of Periodic and Chaos Attractors. When the system is under the conditions that $\xi_1 = 0.1$, $\xi_2 = 0.01$, $\beta = 0.3$, $\varepsilon = 0.6$, $\omega = 1.6$, and $f = 19.5$, the period-3 attractor (A_1) is found to coexist with the chaotic attractor (A_2). Figure 11 presents the time history diagrams of different attractors under the initial conditions of (−1.25, 1, 0, 0) (red curve) and (−1, 1, 0, 0) (blue curve), respectively. As illustrated, A_1 has a higher average amplitude than A_2.

The following conditions are set: matrix $\mathbf{A} = \text{diag}(-10, -10, -10, -10)$ and target orbits $g_1 = 1.25 \sin 0.5t$, $g_2 = 1.25 \cos 0.5t$, $g_3 = 1.25 \sin 0.5t$, and $g_4 = 1.25 \cos 0.5t$. Figure 12 shows the position of the target orbit in the phase space, in which the red areas are the period-3 attractor's basins of attraction, the blue areas are the chaotic attractor's basins of attraction, and the green

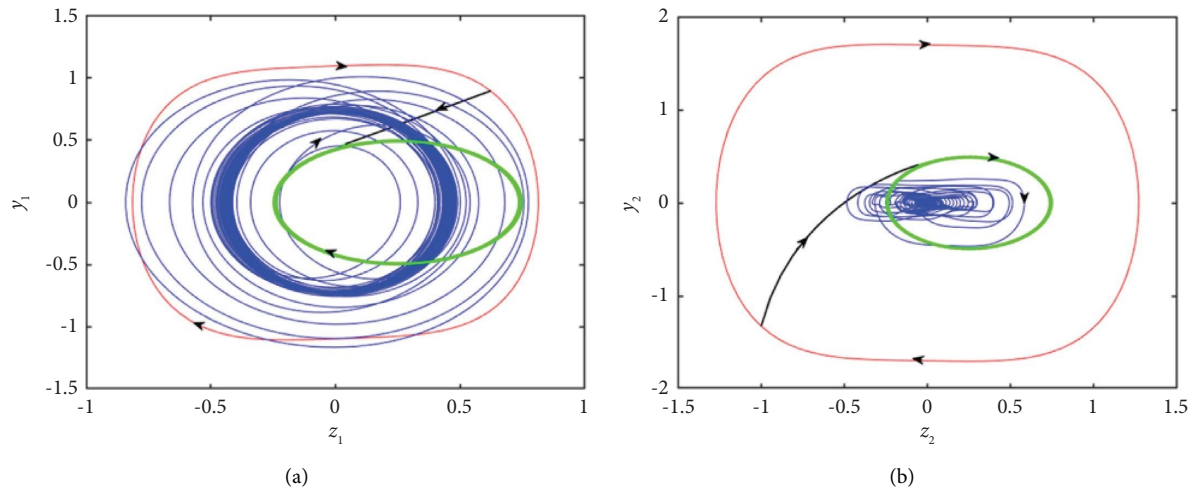

Figure 9: The phase trajectories of the system responses under the OLPNCL control. (a) The mechanical equipment response phase trajectory. (b) The NES response phase trajectory.

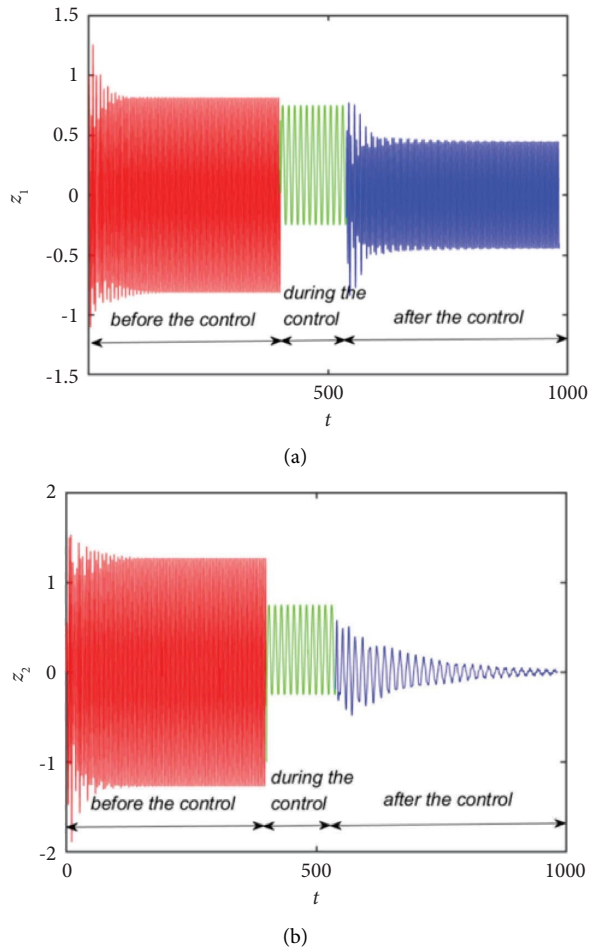

Figure 10: The time history of the system responses under the OLPNCL control. (a) The mechanical equipment vibration response. (b) The NES vibration response.

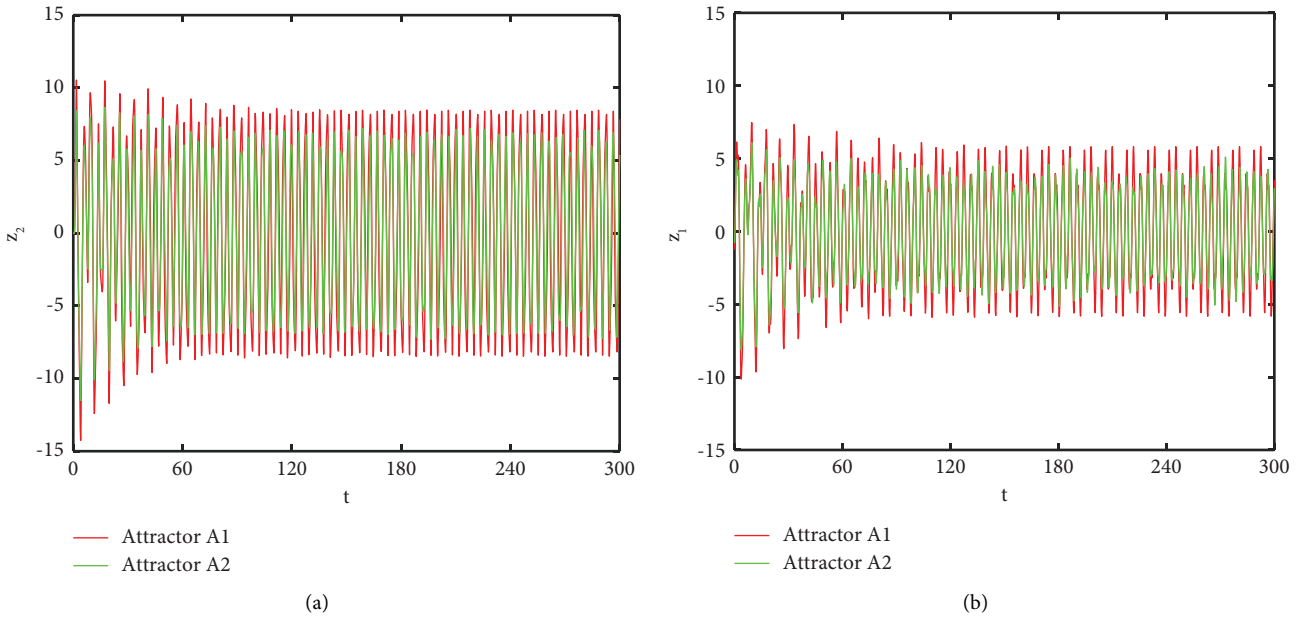

Figure 11: The time history of the system responses under different initial conditions. (a) The mechanical equipment vibration response. (b) The NES vibration response.

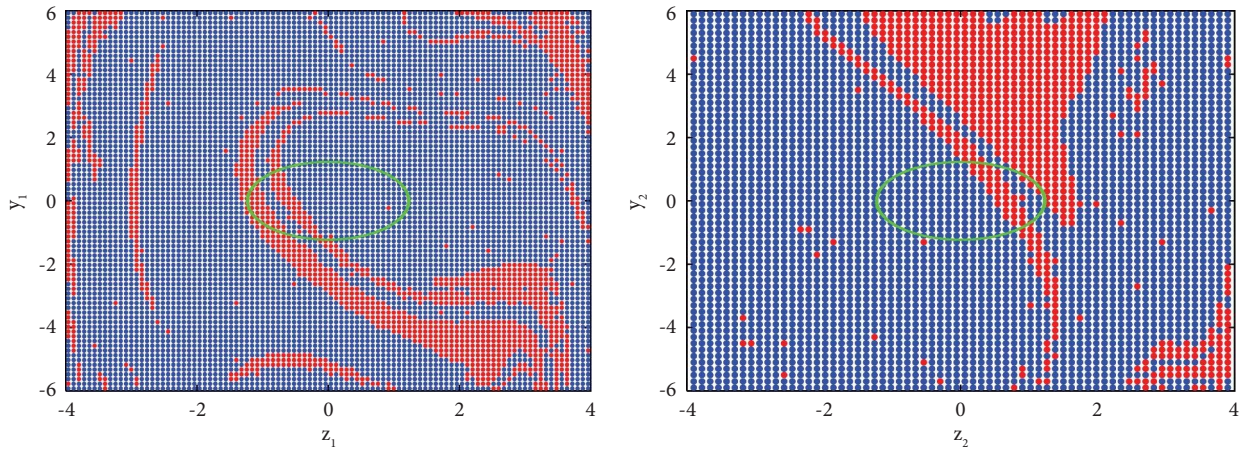

Figure 12: The target orbit's positions in the phase space. (a) The $z_1 - y_1$ analysis plane. (b) The $z_2 - y_2$ analysis plane.

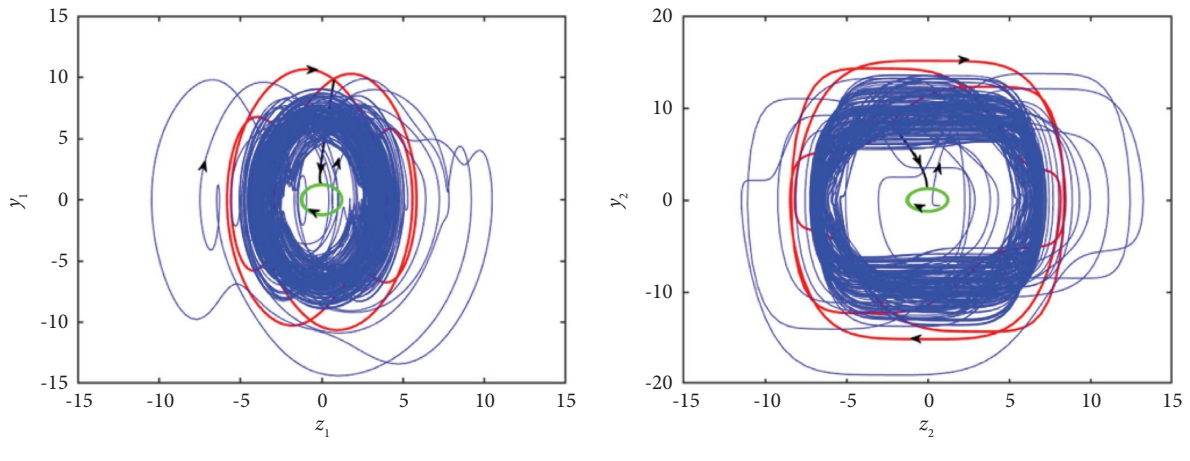

Figure 13: The phase trajectories of the system responses under the OLPNCL control. (a) The mechanical equipment response phase trajectory. (b) The NES response phase trajectory.

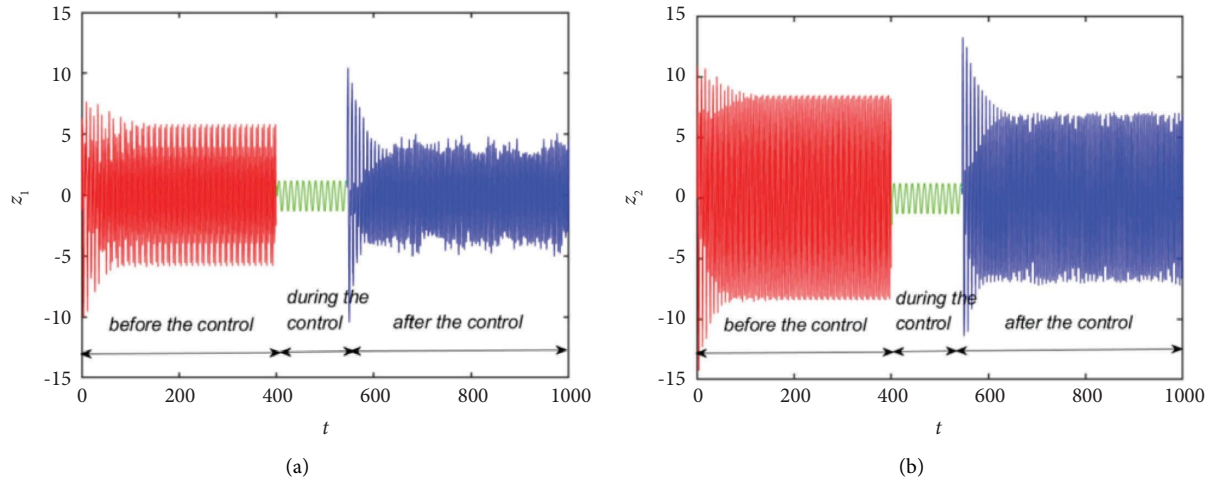

Figure 14: The time history of the system responses under the OLPNCL control. (a) The mechanical equipment vibration response. (b) The NES vibration response.

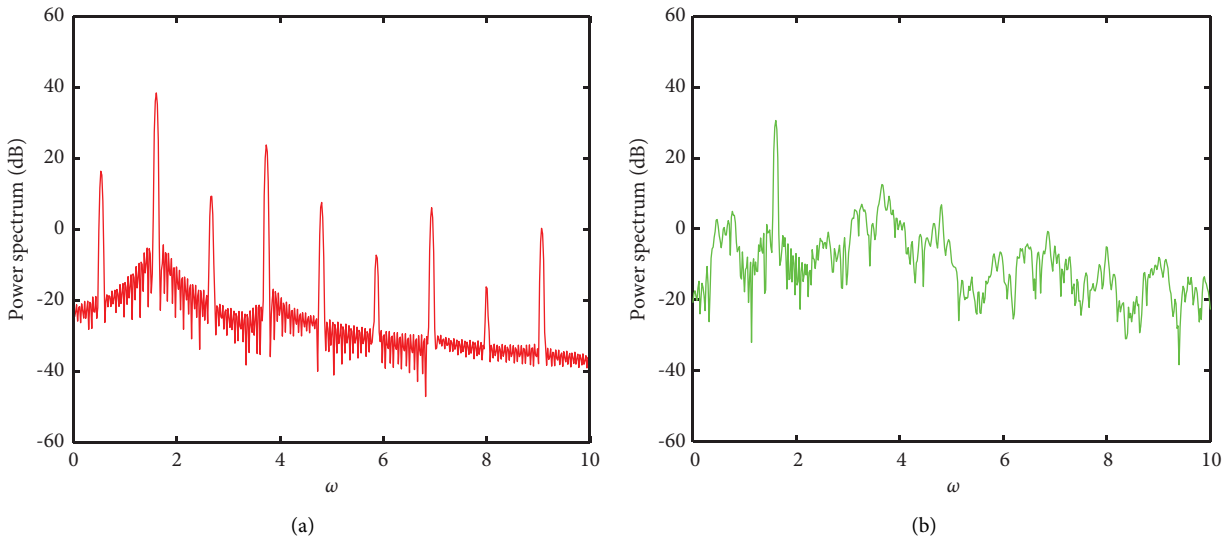

Figure 15: The response power spectrum of the mechanical equipment. (a) No exerting the OLPNCL control. (b) Exerting the OLPNCL control.

curve is the target orbit. It can be seen that the target orbit connects the two attractors' basins of attraction in both the two analysis planes. Figures 13 and 14 present the phase trajectories and time history of the system response during the control process. As illustrated, the OLPNCL method enables the migration from a large-amplitude period 3 attractor to a relatively small-amplitude chaotic attractor.

Figure 15 shows the power spectra of mechanical equipment responses before and after control is applied. As illustrated, when the mechanical equipment is in a state of chaotic motion, the line spectrum components are significantly reduced. Except for the characteristic line spectrum, frequency bands exhibit continuous spectrum characteristics. At the same time, the intensity of the characteristic line spectrum before and after the control which is applied decreases from 38.44 dB to 30.61 dB. Therefore, under this parameter, the OLPNCL method can not only lower the intensity of line spectra but also reconstruct their structure, thereby achieving the dual purpose of reducing the intensity of line spectra while hiding their characteristics.

5. Conclusion

The dynamics model of the NES vibration absorber used for mechanical equipment was built and the global behavior of the model was analyzed by the cell mapping method. The regulations of global features and coexisting multistable attractors were found out, and the OLPNCL migration control algorithm was introduced, achieving migration control of multistable attractors. The main conclusions are as follows:

(1) The NES system exhibited rich dynamic characteristics in a large parameter range, and the coexistence of multiple stable attractors occurred in multiple typical parameter intervals, with complicated global behaviors. In addition, the coexistence of attractors might occur between period and period ($f = 0.68$), period and chaotic attractor ($f = 19.5$), and different attractors were found to have varying amplitudes, which provided prior information for attractor migration control.

(2) The transmission domain of the OLPNCL method was global in the phase space, and the target orbit could be given by an arbitrary vector function connecting two different basins of attraction. Besides, the transmission accuracy was not limited by the polynomial degree of the control equation, and the OLPNCL method was particularly suitable for complex nonlinear systems with the highest polynomial degree $m \geq 3$.

(3) With the OLPNCL method, the migration control of two different types of coexisting attractors was achieved, making the system continuously and stably to operate on a small-amplitude attractor. In particular, when the system response migrated from a large-amplitude periodic attractor to a small-amplitude chaotic attractor, the response characteristic line spectrum intensity of mechanical equipment after the application of the control was reduced from 38.44 dB to 30.61 dB, and the number of line spectra was also significantly lowered. Therefore, the OLPNCL method could not only reduce the intensity of line spectra but also restructure them by taking advantage of the system's chaotic response, thereby achieving the dual purpose of reducing the intensity of line spectra while concealing their characteristics.

Data Availability

The data used to support the findings of this study are available from the corresponding author upon request.

Conflicts of Interest

The authors declare that there are no conflicts of interest regarding the publication of this paper.

Acknowledgments

The study was supported by National Natural Science Foundation of China (Grant no. 51579242), Natural Science Foundation of Hubei Province, China (Grant no. 2018CFB182), and Natural Science Foundation of Hubei Province, China (Grant no. 2022CFB405).

References

[1] S. Sastry, *Nonlinear Systems: Analysis, Stability, and Control*, Springer Science & Business Media, NewYork, NY, USA, 2013.

[2] Y. Sun, J. Xu, G. Lin, and N. Sun, "Adaptive neural network control for maglev vehicle systems with time-varying mass and external disturbance," *Neural Computing & Applications*, pp. 1–12, Springer Science & Business Media, Berlin,Germany, 2021.

[3] F. Liu, D. Yu, C. Wang, and G. Wang, "Advances in variable stiffness vibration isolator and its application in spacecraft," *International Journal of Structural Stability and Dynamics*, vol. 22, no. 13, Article ID 2230004, 2022.

[4] S. S. Oueini and A. H. Nayfeh, "Analysis and application of a nonlinear vibration absorber," *Journal of Vibration and Control*, vol. 6, no. 7, pp. 999–1016, 2000.

[5] R. Ibrahim, "Recent advances in nonlinear passive vibration isolators," *Journal of Sound and Vibration*, vol. 314, no. 3-5, pp. 371–452, 2008.

[6] H. Ding and L. Q. Chen, "Designs, analysis, and applications of nonlinear energy sinks," *Nonlinear Dynamics*, vol. 100, no. 4, pp. 3061–3107, 2020.

[7] J. Chen, W. Zhang, J. Liu, and W. Hu, "Vibration absorption of parallel-coupled nonlinear energy sink under shock and harmonic excitations," *Applied Mathematics and Mechanics volume*, vol. 42, no. 8, pp. 1135–1154, 2021.

[8] Y. Zhang, X. Kong, C. Yue, and H. Xiong, "Dynamic analysis of 1-dof and 2-dof nonlinear energy sink with geometrically nonlinear damping and combined stiffness," *Nonlinear Dynamics*, vol. 105, no. 1, pp. 167–190, 2021.

[9] Z. Miao, Y. Liu, X. Geng, and Y. Lu, "Evaluation of seismic collapse resistance of reinforced concrete frames designed with nonlinear viscous dampers," *Structures*, vol. 40, pp. 960–976, 2022.

[10] M. Mohemmi, E. Mohammadi Dehcheshmeh, and V. Broujerdian, "Seismic vibration control of moment-resistant concrete frames using nonlinear viscous dampers," *Iranian Journal of Science and Technology, Transactions of Civil Engineering*, pp. 1–14, Springer, Berlin,Germany, 2022.

[11] Y. Liu, A. Mojahed, L. A. Bergman, and A. F. Vakakis, "A new way to introduce geometrically nonlinear stiffness and damping with an application to vibration suppression," *Nonlinear Dynamics*, vol. 96, no. 3, pp. 1819–1845, 2019.

[12] G. Habib and G. Kerschen, "A principle of similarity for nonlinear vibration absorbers," *Physica D: Nonlinear Phenomena*, vol. 332, pp. 1–8, 2016.

[13] G. Habib, G. Kerschen, and G. Stepan, "Chatter mitigation using the nonlinear tuned vibration absorber," *International Journal of Non-linear Mechanics*, vol. 91, pp. 103–112, 2017.

[14] B. Lossouarn, J. F. Deü, and G. Kerschen, "A fully passive nonlinear piezoelectric vibration absorber," *Philosophical Transactions of the Royal Society A: Mathematical, Physical & Engineering Sciences*, vol. 376, no. 2127, Article ID 20170142, 2018.

[15] A. F. Vakakis, O. V. Gendelman, L. A. Bergman, D. M. McFarland, G. Kerschen, and Y. S. Lee, *Nonlinear Targeted Energy Transfer in Mechanical and Structural Systems*, Springer Science & Business Media, Berlin, Germany, 2008.

[16] Y. Y. Chen, Z. C. Qian, W. Zhao, and C. M. Chang, "A magnetic Bi-stable nonlinear energy sink for structural seismic control," *Journal of Sound and Vibration*, vol. 473, Article ID 115233, 2020.

[17] Y. Y. Chen, W. T. Su, S. Tesfamariam et al., "Experimental testing and system identification of the sliding bistable nonlinear energy sink implemented to a four-story structure model subjected to earthquake excitation," *Journal of Building Engineering*, vol. 61, Article ID 105226, 2022.

[18] Y. Cao, Z. Li, J. Dou, R. Jia, and H. Yao, "An inerter nonlinear energy sink for torsional vibration suppression of the rotor system," *Journal of Sound and Vibration*, vol. 537, Article ID 117184, 2022.

[19] Y. Cao, H. Yao, H. Li, and J. Dou, "Torsional vibration dynamics of a gear-shafting system attaching a nonlinear energy sink," *Mechanical Systems and Signal Processing*, vol. 176, Article ID 109172, 2022.

[20] J. García Pérez, A. Ghadami, L. Sanches, G. Michon, and B. I. Epureanu, "Data-driven optimization for flutter suppression by using an aeroelastic nonlinear energy sink," *Journal of Fluids and Structures*, vol. 114, Article ID 103715, 2022.

[21] J. Zhou, M. L. Xu, Z. C. Yang, and Y. S. Gu, "Suppressing nonlinear aeroelastic response of laminated composite panels in supersonic airflows using a nonlinear energy sink," *Chinese Journal of Aeronautics*, vol. 34, no. 2, pp. 376–385, 2021.

[22] D. Zou, G. Liu, Z. Rao, T. Tan, W. Zhang, and W. H. Liao, "A device capable of customizing nonlinear forces for vibration energy harvesting, vibration isolation, and nonlinear energy sink," *Mechanical Systems and Signal Processing*, vol. 147, Article ID 107101, 2021.

[23] J. Zang, R. Q. Cao, Y. W. Zhang, B. Fang, and L. Q. Chen, "A lever-enhanced nonlinear energy sink absorber harvesting vibratory energy via giant magnetostrictive-piezoelectricity," *Communications in Nonlinear Science and Numerical Simulation*, vol. 95, Article ID 105620, 2021.

[24] D. Dudkowski, S. Jafari, T. Kapitaniak, N. V. Kuznetsov, G. A. Leonov, and A. Prasad, "Hidden attractors in dynamical systems," *Physics Reports*, vol. 637, pp. 1–50, 2016.

[25] A. N. Pisarchik and A. E. Hramov, *Multistability in Physical and Living Systems*, Springer Nature Switzerland AG, Cham, Switzerland, 2022.

[26] J. Wang and X. Wang, "A global control of polynomial chaotic systems," *International Journal of Control*, vol. 72, no. 10, pp. 911–918, 1999.

[27] Y. Starosvetsky and O. V. Gendelman, "Vibration absorption in systems with a nonlinear energy sink: nonlinear damping," *Journal of Sound and Vibration*, vol. 324, no. 3-5, pp. 916–939, 2009.

[28] R. P. Eason, *High amplitude response behavior of a linear oscillator–nonlinear absorber system: identification, analysis, and attenuation by using a semi-active absorber in series*, PHD Thesis, Rice University, Houston TX,USA, 2013.

[29] J. Zang, T. C. Yuan, Z. Q. Lu, Y. W. Zhang, H. Ding, and L. Q. Chen, "A lever-type nonlinear energy sink," *Journal of Sound and Vibration*, vol. 437, pp. 119–134, 2018.

[30] C. S. Hsu and R. S. Guttalu, "An unravelling algorithm for global analysis of dynamical systems: an application of cell-to-cell mappings," *Journal of Applied Mechanics*, vol. 47, no. 4, pp. 940–948, 1980.

[31] E. Kreuzer and B. Lagemann, "Cell mappings for multi-degree-of-freedom-systems—parallel computing in nonlinear dynamics," *Chaos, Solitons & Fractals*, vol. 7, no. 10, pp. 1683–1691, 1996.

[32] F. R. Xiong, Z. C. Qin, Q. Ding et al., "Parallel cell mapping method for global analysis of high-dimensional nonlinear dynamical systems," *Journal of Applied Mechanics*, vol. 82, no. 11, Article ID 111010, 2015.

[33] K. Chai, S. Li, J. J. Lou, X. Yu, Y. S. Liu, and C. Q. Yang, "Line spectra chaotification of the nonlinear vibration isolation system on the flexible foundation based on the open-plus-nonlinear-closed-loop method," *Journal of Vibration and Control*, vol. 27, no. 7-8, pp. 731–742, 2021.